Progress In Electromagnetics Research C, Vol. 121, 83–95, 2022

Correlation between Elements of a Massive MIMO Antenna in a Sub-6 GHz Mobile Terminal

Ahmed M. Elshirkasi[1], Azremi Abdullah Al-Hadi[1, *], Rizwan Khan[2], and Ping Jack Soh[1, 3]

Abstract—This work studies the correlation between 14-elements of a sub-6 GHz MIMO antenna for mobile terminal, operating in the 3.10 to 3.85 GHz frequency band. Envelope correlation coefficient (ECC) was used to assess the relationship between MIMO antenna elements. A total of 91 ECC values were considered at every frequency point for the 14-element antenna, which was performed under two propagation scenarios: (i) a uniform environment, and (ii) a Gaussian environment. For the latter, three angular spreads (AS) of 20°, 30°, and 40° and incident angle of every 10° in both elevation and azimuth coordinates are considered. The resulting ECC in the uniform environment is below 0.15 over the entire operating frequency band, indicating that the 14 elements are minimally correlated. However, in a Gaussian environment, the ECC is evaluated at 3.25 GHz. For the AS values of 20°, 30°, and 40°. The average number of ECC values below the 0.3 threshold is 48, 67, and 81 out of 91 total ECC values, respectively. Finally, a relation is derived between the number of ECC values below 0.3 and the lowly-correlated number of antenna elements. It is seen that at a wider angular spread of 40°, the number of equivalent lowly-correlated elements is 12 with 87% from all considered incident wave directions.

1. INTRODUCTION

The fifth generation (5G) of mobile communication is aimed at providing higher capacity, low latency, increased reliability, and support massive number of connected devices [1, 2]. Operating using MIMO technology and antennas on both sides of the link is one of the key enablers to support high data rates and improve immunity to interference without requiring more bandwidth or transmit power [3]. MIMO antenna elements on mobile terminals should be highly efficient, small in size, low in cost, and strategically placed on the device chassis [4, 5]. Furthermore, the correlation between these elements should be low for the channels to be independent and thus, enable a system with high capacity [6]. The correlation between MIMO antenna elements is defined by the envelope correlation coefficient (ECC) with a threshold of 0.5 and is then reduced to less than 0.3 in 4G systems [7].

The integration of two and four antenna elements on a mobile terminal has been proven to be sufficient to meet the performance requirements of 3G and 4G mobile communication systems [8, 9]. However, more antenna elements are required to meet the desired performance in a 5G system, but this is limited to the available space on the chassis [10]. Moreover, the number of antenna elements on a mobile terminal increases the required amount of circuitry and signal processing capability [11]. Several sub-6 GHz MIMO antennas for mobile terminal with large number of elements have been reported in the literature. For instance, a 10-element MIMO antennas in [12–14], a 12-element MIMO antenna in [15] and [16], 14-element and 16-element MIMO antennas in [17] and [18], respectively. Up to a 20-element

Received 31 March 2022, Accepted 9 June 2022, Scheduled 30 June 2022

* Corresponding author: Azremi Abdullah Al-Hadi (azremi@unimap.edu.my).

[1] Advanced Communication Engineering (ACE) Center of Excellence, Faculty of Electronic Engineering Technology (FTKEN), Universiti Malaysia Perlis, Kangar 01000, Perlis, Malaysia. [2] Department of Research and Development, Laird Technologies (M) SdnBhd, Perai 13600, Penang, Malaysia. [3] Centre for Wireless Communications (CWC), University of Oulu, Oulu 90570, Finland.

Table 1. Reported ECC values of MIMO antennas with large number of elements on mobile terminal.

References	Number of antenna elements	Frequency bands	ECC
[25]	8	Lower Band (LB): 3.4–3.6 GHz Upper Band (UB): 4.8–5.1 GHz	< 0.10
[26]	10	Lower Band (LB): 3.4–3.8 GHz Upper Band (UB): 5.150–5.925 GHz	< 0.15
[15]	12	8 elements to operate on LTE bands42/43 3.4–3.8 GHz 6 elements to operate on LTE band 46 5.150–5.925 GHz	< 0.10
[27]	14	Lower Band (LB): 3.10–3.85 GHz Upper Band (UB): 5.60–7.20 GHz	< 0.15
[28]	16	5–6 GHz	< 0.31
[29]	18	LTE Bands 42/43: 3.4–3.8 GHz	< 0.10
[19]	20	3.4–3.6 GHz	< 0.10

MIMO antenna for mobile terminal was proposed in [19]. Table 1 lists 5G MIMO antenna for mobile terminals with large number of elements. The ECC values of these antennas are listed and all within or close to the threshold of the 0.3.

Besides considerations on hardware complexity, the performance of MIMO antennas on mobile terminals can degrade in practice for a variety of reasons, including the effects of a user's body and the propagation environment. A mobile terminal used in close proximity to the user's body may results in blocking the antenna elements, degrading the performance of the wireless link [20]. On the other hand, a widely adopted assumption when evaluating the performance of MIMO antennas is that the antenna is operating in a uniform environment. However, the incident signal in practical cellular propagation environments originate from specific directions, limiting the performance of MIMO antennas designed with this assumption on a mobile terminal. Thus, the ECC of MIMO antennas with large number of elements for mobile terminal needs to be investigated in directive environments. Directive propagation environments are modeled as Gaussian or Laplacian, with limited angular spread (AS) [21, 22]. The measurement-based wireless channel model WINNER-II considers the angular spread of the signal at the mobile terminal in different propagation indoor and outdoor scenarios to be 12° and 53° [23, 24].

This work investigates the correlation in a 14-element sub-6 GHz band MIMO antenna operating in the uniform and a directive propagation environment, which is characterized by ECC. The directive environment is modeled as Gaussian distribution in both elevation and azimuth planes. In addition to that, a relationship between the number of ECC values below the threshold of 0.3 and the number of antenna elements is used to find the equivalent MIMO system with lowly-correlation elements. The study's uniqueness stems from its examination of the relationship between a large number of elements of a sub-6 GHz mobile terminal MIMO antenna in both directive and uniform environments.

The article is organized as follows. Section 2 presents the details of the 14-element MIMO antennas and its performance. Next, Section 3 discusses ECC calculations and numerical methods as well as the model of the Gaussian distributed propagation environment. Section 4 presents the results and discussion. Finally, Section 5 concludes the work.

2. MIMO ANTENNA DESIGN

In this work, we use the design of MIMO antenna from [27], which has 14 identical two-branch monopoles and operates in two bands. They are placed symmetrically around a plane of a metallic ground and

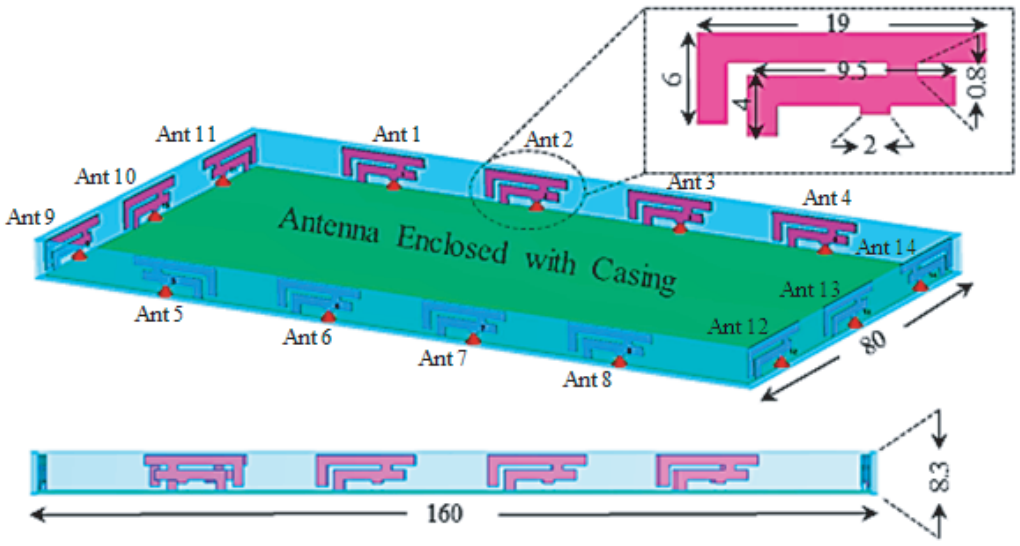

Figure 1. The 14 antenna elements placed on a chassis and enclosed with a casing. Dimensions are in mm.

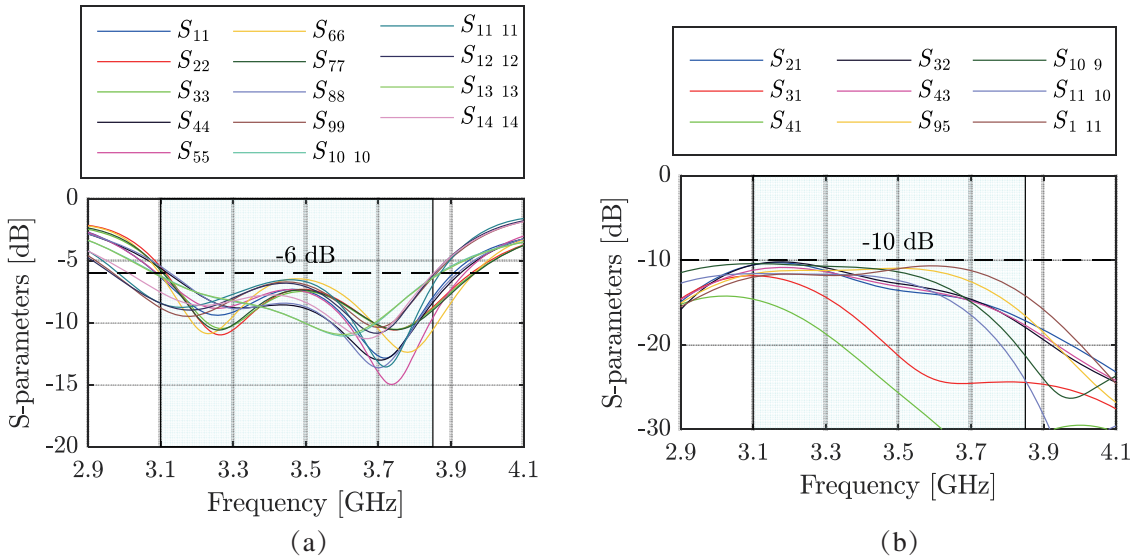

Figure 2. Simulated reflection coefficients of the antenna. (a) Reflection coefficient. (b) Isolation (dB).

enclosed with a casing as shown in Figure 1. However, we selected the lower sub-6 GHz band which operates from 3.10 to 3.85 GHz (LTE bands 42 and 43) for the study in this work. The S-parameter of the lower band is shown in Figure 2.

Figure 3 depicts the 3D radiation pattern of antenna element 1 at 3.25 GHz in both horizontal and vertical polarizations, as an example. For this same element and at the same frequency, its 2D radiation pattern sliced in the xy-plane is depicted in Figure 4.

The efficiency of the 14 elements is depicted in Figure 5. All elements are similar in their increasing/decreasing efficiency behavior with frequency. Furthermore, the efficiency values range from 41% to 77%. An average efficiency for all antenna elements is also calculated in this figure, which varies between 47% and 71% depending on frequency.

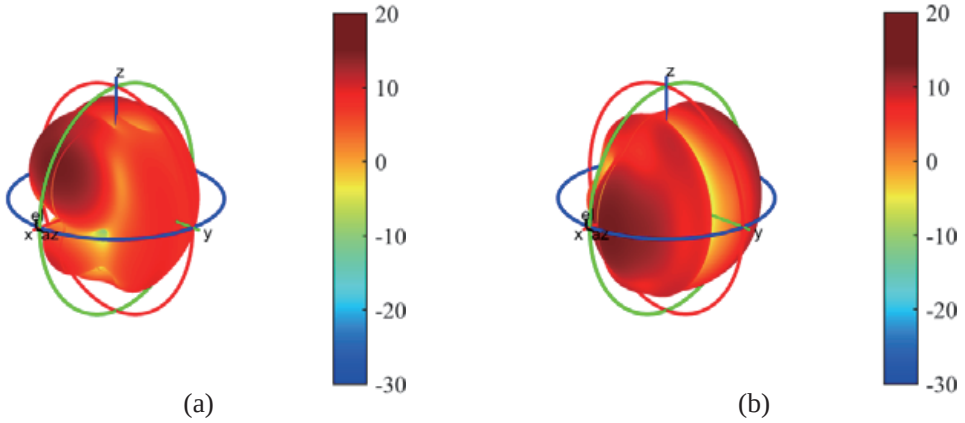

Figure 3. 3D radiation pattern of the antenna element 1 at 3.25 GHz. (a) Horizontal polarization. (b) Vertical polarization.

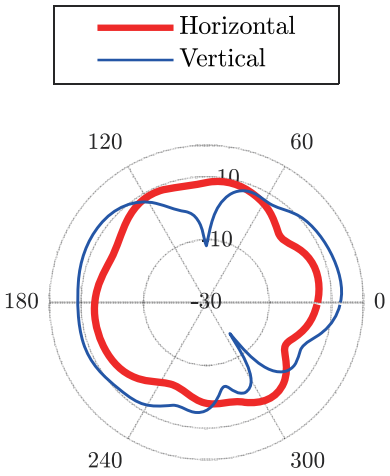

Figure 4. 2D radiation pattern of antenna element 1 in the x-y plane of both horizontal and vertical polarizations.

3. ECC CALCULATIONS

For a MIMO antenna of M elements, there are N_{ECC} values at every simulated or measured frequency point, as follows:

$$N_{ECC} = \frac{M(M-1)}{2} \tag{1}$$

Thus, for the 14-element MIMO antenna in this study, there will be 91 ECC values at each simulation frequency point.

ECC between antenna elements i and $j(\rho_{e,ij})$ can be calculated using a simple S-parameter formula presented in [30] for a two port MIMO antenna, which can then be generalized for any number of ports M in [31]. The ECC between ports i and j can be calculated using the method as follows:

$$\rho_{e,ij} = \left| \frac{-\sum_{n=1}^{M} S_{ni}^{*} S_{nj}}{\sqrt{\left(1 - \sum_{n=1}^{M} |S_{ni}|^2\right)\left(1 - \sum_{n=1}^{M} |S_{nj}|^2\right)}} \right|^2 \tag{2}$$

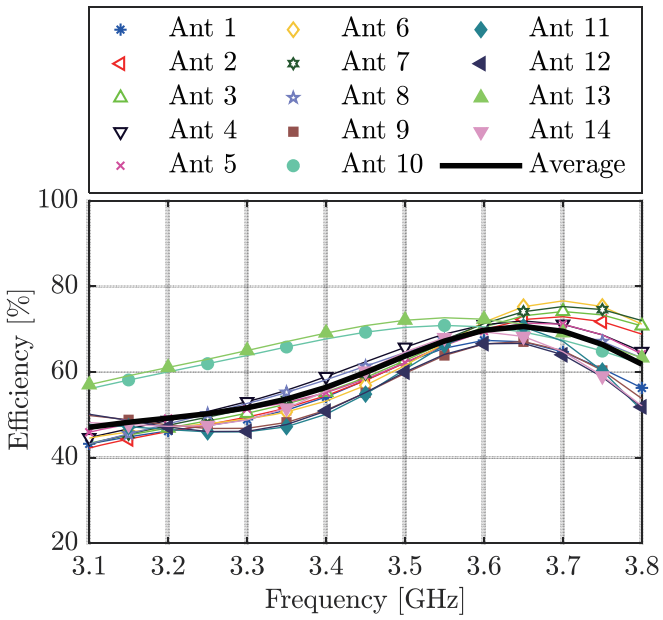

Figure 5. Efficiency of the 14 elements.

where S_{ni} and S_{nj} are the S-parameters between ports i and j and the other ports. However, this formula produces accurate results only if the total radiation efficiency of the antenna elements is 100%, which is not the case in real-world antenna designs; otherwise, it underestimates the ECC and should be avoided [32]. The formula of the complex far-field radiation pattern yields accurate ECC results, which are as follows [33]:

$$\rho_{e,ij} = \left| \frac{\int_0^{2\pi}\int_0^{\pi}\left(XPR\cdot E_{\theta i}(\theta,\phi)\cdot E^*_{\theta j}(\theta,\phi)\cdot P_\theta(\theta,\phi) + XPR\cdot E_{\phi i}(\theta,\phi)\cdot E^*_{\phi j}(\theta,\phi)\cdot P_\phi(\theta,\phi)\right)\sin(\theta)\,d\theta d\phi}{\sqrt{\prod_{k=i,j}\int_0^{2\pi}\int_0^{\pi}\left(XPR\cdot E_{\theta k}(\theta,\phi)\cdot E^*_{\theta k}(\theta,\phi)\cdot P_\theta(\theta,\phi)+XPR\cdot E_{\phi k}(\theta,\phi)\cdot E^*_{\phi k}(\theta,\phi)\cdot P_\phi(\theta,\phi)\right)\sin(\theta)d\theta d\phi}} \right|^2 \tag{3}$$

where $XPR = P_V/P_H$ denotes to the cross discrimination ratio between vertical and horizontal polarized power components, and $E_{\theta i}(\theta\phi)$, $E_{\theta j}(\theta\phi)$, $E_{\phi i}(\theta\phi)$, $E_{\phi j}(\theta\phi)$ are the field components of i and j ports in elevation and azimuth polarizations, respectively. $(\cdot)^*$ is the conjugate operator. $P_\theta(\theta\phi)$ and $P_\phi(\theta\phi)$ are the elevational and azimuthal angular power spectrum (APS) which should fulfill the normalization condition as follows:

$$\int_0^{2\pi}\int_0^{\pi} P_\theta(\theta,\phi)\sin(\theta)\,d\theta d\phi = 1, \quad \int_0^{2\pi}\int_0^{\pi} P_\phi(\theta,\phi)\sin(\theta)\,d\theta d\phi = 1 \tag{4}$$

In addition to its accuracy, the radiation pattern formula can account for the propagation environment distribution. When the incident signal is assumed to come from all directions equally, the environment can be modeled as a uniform distribution. In this case, both $P_\theta(\theta\phi)$ and $P_\phi(\theta\phi)$ are $1/4\pi$.

On the other hand, when the signal is assumed to come from a specific direction, the propagation environment distribution can be modeled as Gaussian or Laplacian distribution. In this work, we follow the propagation environment model described in [21, 24, 34], in which $P_\theta(\theta\phi)$ and $P_\phi(\theta\phi)$ are modeled as Gaussian in both the elevation and azimuth planes, as follows [35, 36]:

$$P_\theta(\theta,\phi) = P_\phi(\theta,\phi) = A_0 w_\theta w_\phi, \quad 0 \le \theta < \pi, \quad 0 \le \phi < 2\pi \tag{5}$$

w_θ and w_ϕ are the elevational and azimuthal polarised components, which are modeled as Gaussian distribution as shown below:

$$w_\theta = \exp\left(-\frac{(\theta-\mu_\theta)^2}{2\sigma_\theta^2}\right)$$
$$w_\phi = \exp\left(-\frac{(\phi-\mu_\phi)^2}{2\sigma_\phi^2}\right) \tag{6}$$

where μ_θ, σ_θ, μ_ϕ and σ_ϕ are the mean values and the standard deviations of the Gaussian distributions in elevation and azimuth, respectively. A_0 is a constant to fulfill the normalization condition of the APS. The direction of the incident wave in elevation and azimuth planes is controlled by μ_θ and μ_ϕ respectively, while σ_θ and σ_ϕ represent the angular spectrum of the signal AS in elevation and azimuth, respectively. The elevation-azimuth coordinates are shown in Figure 6.

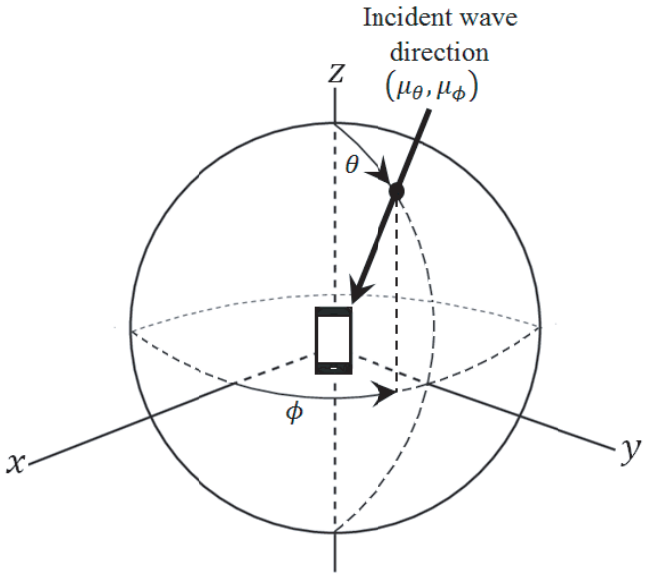

Figure 6. The incident wave direction in elevation-azimuth plane.

For numerical calculations, the far-field radiation pattern of MIMO ports is simulated or measured at discreet angles along elevation and azimuth planes. This allows $\theta_0, \theta_1, \ldots, \theta_{n_\theta-1}$ and $\phi_0, \phi_1, \ldots, \phi_{n_\phi-1}$ to be the discrete angles in elevation and azimuth planes over 0 to π and 0 to 2π and with step size $\Delta\theta$ and $\Delta\phi$, respectively. At these angles, the field components in (3), namely $(E_{\theta i}, E_{\theta j}E_{\phi i}, E_{\phi j})$, can be written in a matrix of size $n_\theta \times n_\phi$. For example, the field component $\mathbf{E}_{\theta_i}$ can be written as [34]:

$$\mathbf{E}_{\theta_i} = \begin{bmatrix} E_{\theta i}^{\theta_0,\phi_0} & E_{\theta i}^{\theta_0,\phi_2} & \cdots & E_{\theta i}^{\theta_0,\phi_{n_\phi-1}} \\ E_{\theta i}^{\theta_1,\phi_0} & E_{\theta i}^{\theta_1,\phi_2} & \cdots & E_{\theta i}^{\theta_2,\phi_{n_\phi-1}} \\ \vdots & \vdots & \cdots & \vdots \\ E_{\theta i}^{\theta_{n_\theta-1},\phi_0} & E_{\theta i}^{\theta_{n_\theta-1},\phi_2} & \cdots & E_{\theta i}^{\theta_{n_\theta-1},\phi_{n_\phi-1}} \end{bmatrix} \tag{7}$$

w_θ and w_ϕ of the Gaussian APS are calculated at discrete values of θ and ϕ as follows:

$$\mathbf{w}_\theta = \begin{bmatrix} w_\theta^{\theta_0} & w_\theta^{\theta_1} & \cdots & w_\theta^{\theta_{n_\theta-1}} \end{bmatrix}^T$$
$$\mathbf{w}_\phi = \begin{bmatrix} w_\phi^{\phi_0} & w_\phi^{\phi_1} & \cdots & w_\phi^{\phi_{n_\phi-1}} \end{bmatrix}^T \tag{8}$$

then the APS at each spatial point (θ, ϕ) in the elevation-azimuth plane is formed as:

$$\mathbf{P}_{\theta}^{m,n} = \mathbf{P}_{\phi}^{m,n} = A_0 \mathbf{w}_{\theta} \mathbf{w}_{\phi}^{\mathbf{T}} \tag{9}$$

where $m = 0, 1, 2, \ldots, n_\theta$, and $n = 1, 2, 3, \ldots, n_\phi$.

Finally, substituting discrete forms of pattern fields and APSs in the ECC equation and replacing the integral with a summation operation over the two dimensions of the elevation-azimuth plane yields the following final calculation formula:

$$\rho_{e,ij} = \left| \frac{\sum_{m=0}^{n_\theta-1} \sum_{n=0}^{n_\phi-1} \left(XPR \cdot \mathbf{E}_{\theta i}^{m,n} \cdot \left(\mathbf{E}_{\theta j}^{m,n} \right)^* \cdot \mathbf{P}_{\theta}^{m,n} + XPR \cdot \mathbf{E}_{\phi i}^{m,n} \cdot \left(\mathbf{E}_{\phi j}^{m,n} \right)^* \cdot \mathbf{P}_{\phi}^{m,n} \right) \cdot \sin(\theta^m) \cdot \Delta\theta \cdot \Delta\phi}{\sqrt{\prod_{k=i,j} \sum_{m=0}^{n_\theta-1} \sum_{n=0}^{n_\phi-1} \left(XPR \cdot \mathbf{E}_{\theta k}^{m,n} \cdot \left(\mathbf{E}_{\theta k}^{m,n} \right)^* \cdot \mathbf{P}_{\theta}^{m,n} + XPR \cdot \mathbf{E}_{\phi k}^{m,n} \cdot \left(\mathbf{E}_{\phi k}^{m,n} \right)^* \cdot \mathbf{P}_{\phi}^{m,n} \right) \cdot \sin(\theta^m) \cdot \Delta\theta \cdot \Delta\phi}} \right|^2 \tag{10}$$

The simulation parameters in this work are listed in Table 2.

Table 2. Parameters of ECC calculations in this work.

Parameter		Value
XPR		0 dB (1)
Frequency	Uniform environment	3.1–3.8 GHz
	Gaussian environment	3.25 GHz
Direction of the incident signal	μ_θ	Every 10° in the elevation coordinate.
	μ_ϕ	Every 10° in the azimuth coordinate.
Angular spread of the incident signal	σ_θ	20°, 30°, 40°.
	σ_ϕ	20°, 30°, 40°.

4. RESULTS AND DISCUSSION

ECC values under the assumption of a uniform environment are depicted in Figure 7, and the maximum ECC value among the 91 ECCs at each simulation frequency point is depicted in this figure. The ECC values are all below the 0.3 threshold, with the highest value being 0.15. This indicates that in a uniform environment, the antenna elements are highly uncorrelated.

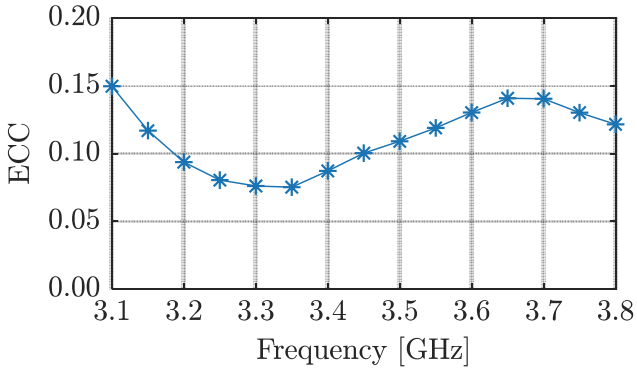

Figure 7. Maximum ECC at every simulation frequency point in a uniform environment.

Next, the ECC is calculated under the assumption of a Gaussian distributed propagation environment. All ECC calculations are performed at the center frequency of 3.25 GHz and at three

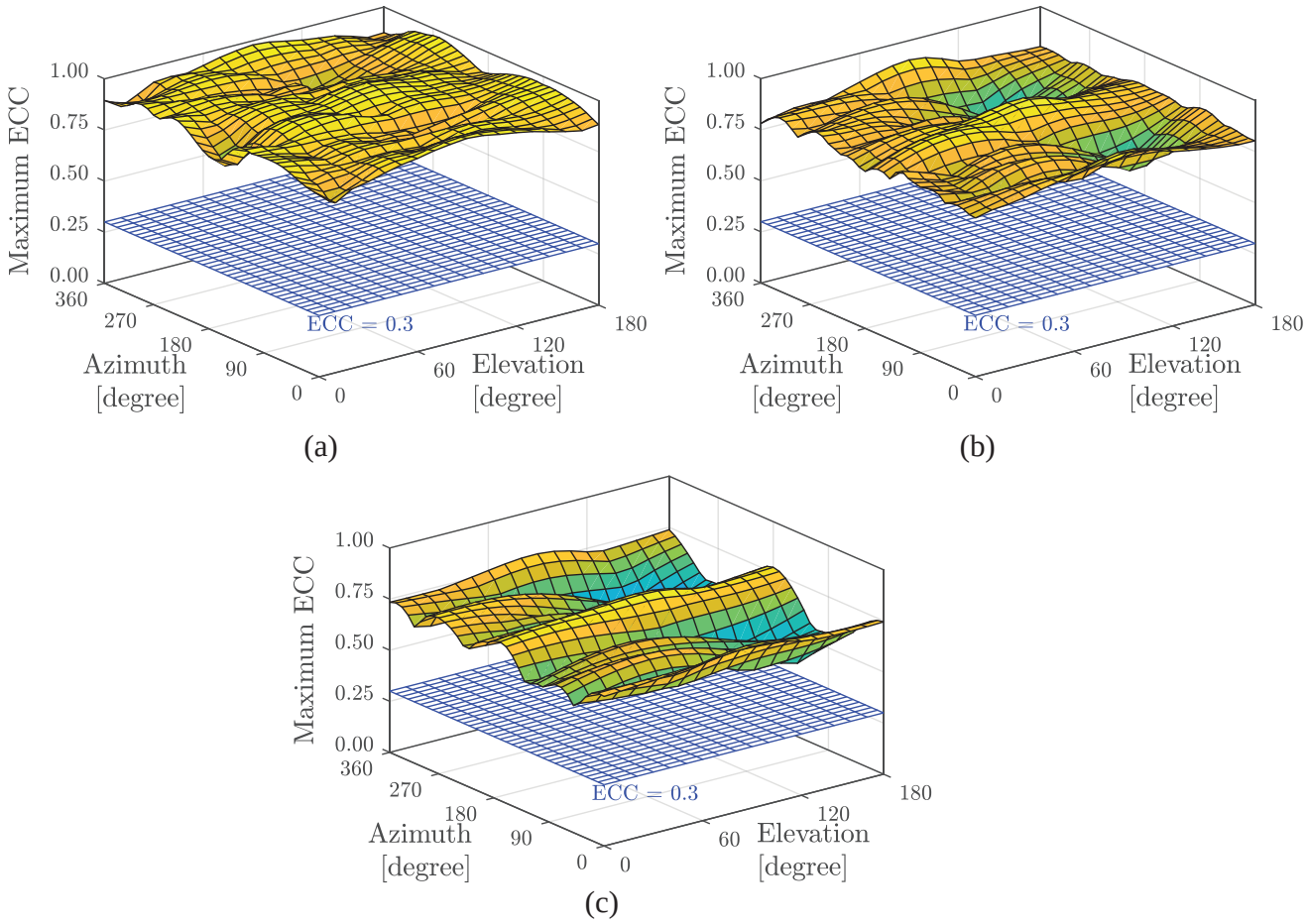

Figure 8. Maximum ECC at every incident direction of the directive environment with three AS values. (a) Angular spread AS = 20. (b) Angular spread AS = 30. (c) Angular spread AS = 40.

different angular spread namely 20°, 30°, 40°. The maximum ECC at each incident direction in the three AS values is shown in Figure 8, with the reference ECC level of 0.3 shown. In general, it is seen that the maximum ECC at every incident direction is above the 0.3 threshold, and it near the unity. Furthermore, the narrower the AS is, the higher the ECC is.

When the AS is set to 20°, the maximum ECC values range is from 0.76 to 0.98, with an average of 0.92. As the AS is increased to 30°, the values decrease; in this case, the maximum ECC values range is from 0.61 to 0.91, with an average of 0.80. As the AS is widened to 40°, the ECC improves even more, with maximum ECC values ranging from 0.48 to 0.81 and an average value of 0.67.

The effect of the environment is clearly visible when comparing maximum ECC values in a uniform and a Gaussian distributed propagation environment, as shown in Figure 7 and Figure 8, respectively. The ECC increases when the incident signal originates from specific direction with a narrow angular spread and not uniformly from all directions. However, considering only the maximum ECC at each incident direction does not provide a clear view on the other ECC values in the same direction of incidence. Figure 9 depicts the number of ECC values that are below the 0.3 threshold at every incident direction in the elevation-azimuth plane.

There is a clear improvement in performance with wider AS values, as evidenced by the increasing number of ECCs being below 0.3. When the AS is 20°, the number of ECCs below the threshold ranges from 26 to 72, with an average of 48. The ECC is clearly dependent on the direction of the incident wave in this narrow propagation environment scenario. There is an increase in the number of ECCs which are within the acceptable range with an AS of 30°. The number of ECCs < 0.3 in this case ranging from 49 to 77, with a mean of 67, and the dependence on direction is lesser with this AS (30°)

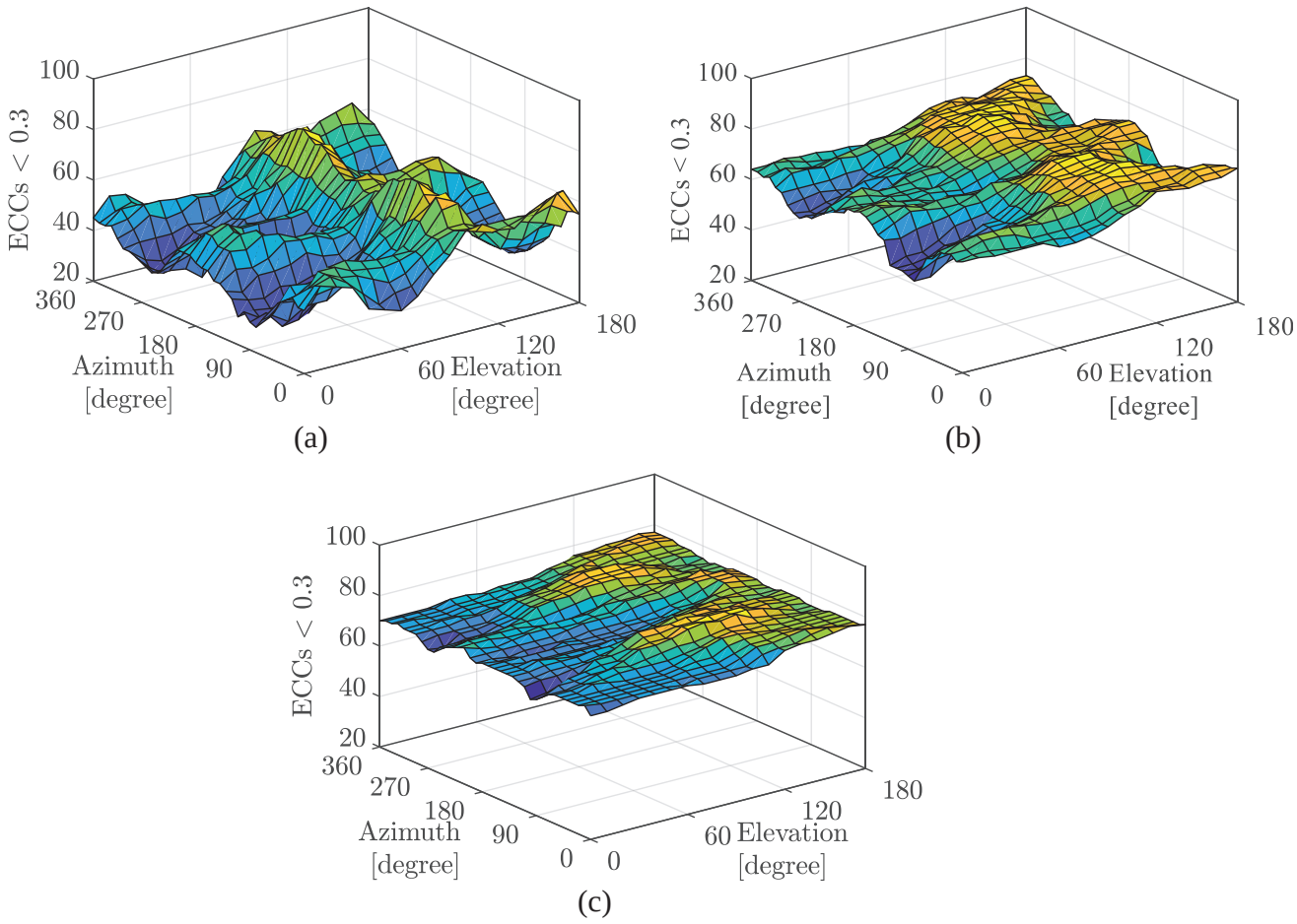

Figure 9. Number of ECCs < 0.3 at every incident direction of the directive environment with three AS values. (a) Angular spread AS $= 20$. (b) Angular spread AS $= 30$. (c) Angular spread AS $= 40$.

than with the previous AS (20°). Finally, the AS is set to 40, which results in a greater number of ECCs below the 0.3 threshold, with a mean value of 74 and limits between 65 and 81. Furthermore, the impact of the incident direction is reduced as the numbers get closer in all directions.

Next, the number of ECCs below the threshold of 0.3 is linked with the number of antenna elements that are lowly-correlated. This is done by replacing N_{ECC} in (1) by $N_{ECC<0.3}$ and solving it for number of antenna elements with ECC < 0.3. Solving (1) for M as gives:

$$M^2 - M - 2N_{ECC<0.3} = 0 \tag{11}$$

This equation has two roots; a negative root which is neglected, and a positive root from which the equivalent number of uncorrelated antenna elements M_{eq} is deduced as follows:

$$M_{eq} = \lfloor r \rfloor = \frac{1 + \sqrt{1 + 8N_{ECC<0.3}}}{2} \tag{12}$$

where r is the positive root, and $\lfloor x \rfloor$ denotes rounding x to the nearest lower integer to obtain an integer number of antenna elements.

The number of antenna elements in (12) is shown in Figure 10. In general, increasing the width of the incident wave leads to a higher number of lowly-correlated antenna elements, as well as less independence from the incident direction. This is also affirmed from the results in Figure 9. When the incident signal's angular spread is set to 20°, the lowest number of lowly-correlated elements is 7, and the highest number is 12, with values varying based on the different directions of the incident signal. When the angular spread is increased to 30°, a higher number of lowly-correlated elements (between

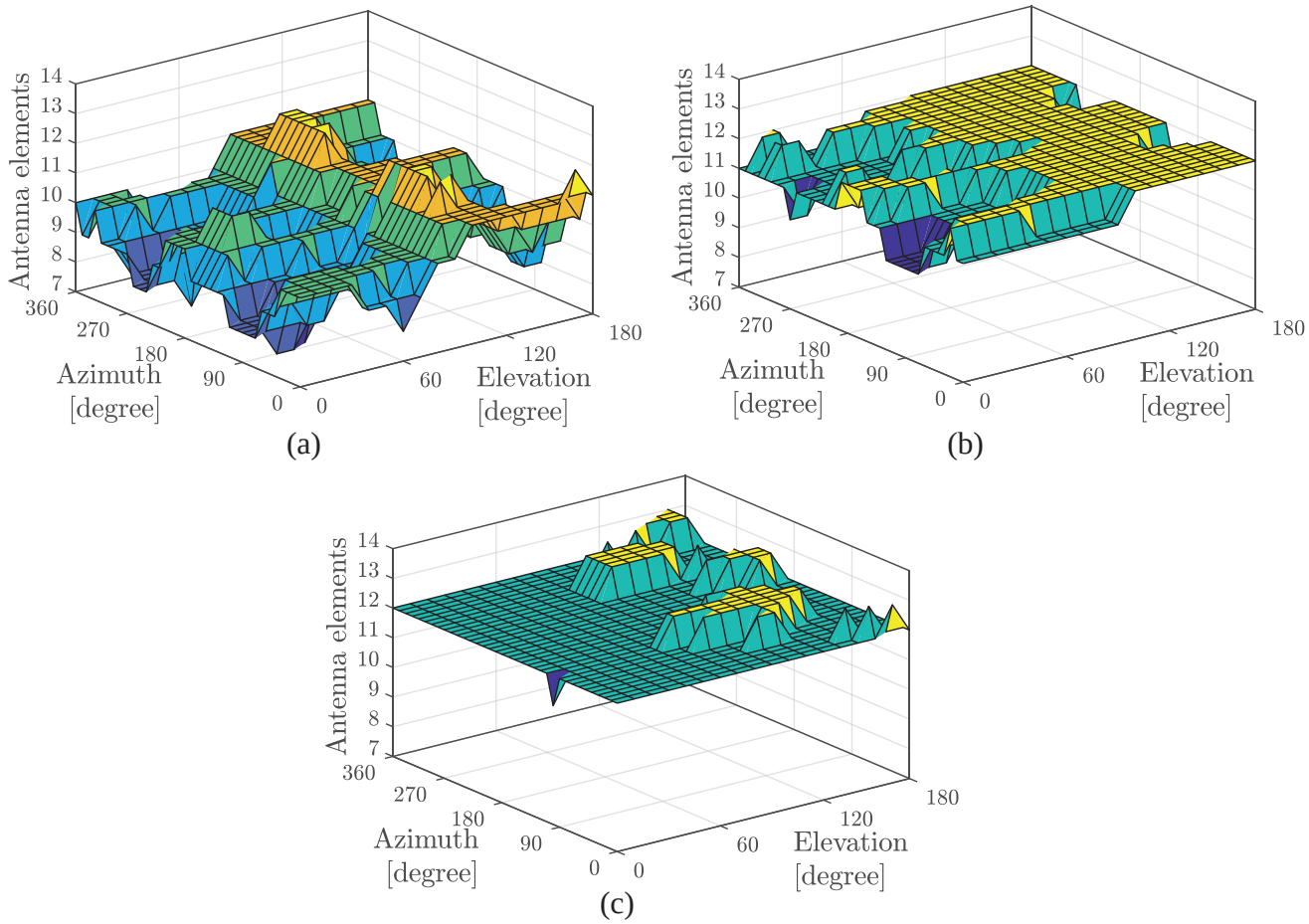

Figure 10. Number of lowly-correlated antenna elements at every incident directions of the directive environment at the three AS values. (a) Angular spread AS = 20. (b) Angular spread AS = 30. (c) Angular spread AS = 40.

10 and 12) is achieved. There is more stability in all directions with this angular spread. When the angular spread is extended to 40°, the highest number of lowly-correlated elements is obtained, which ranges from 12 to 13. This system, however, still did not achieve the desired low correlation criteria for all elements even at this angular spread.

Finally, the statistical distribution of the number of lowly-correlated elements is shown in Figure 11. The distribution of antenna elements from all directions is depicted in this diagram for each angular spread value. When the angular spread is set to 20°, the most lowly-correlated numbers of elements are

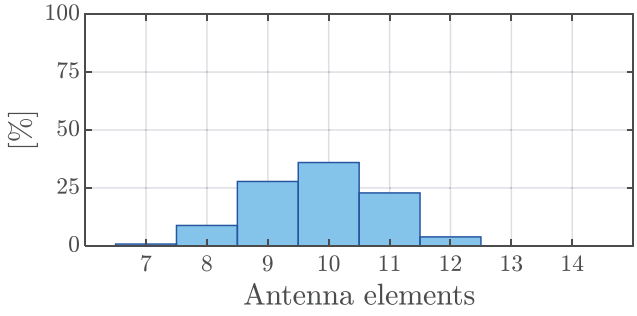

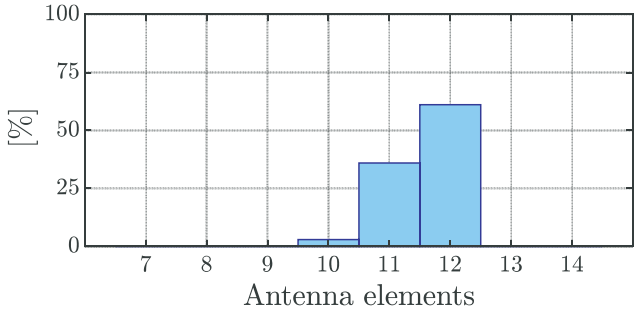

(b)

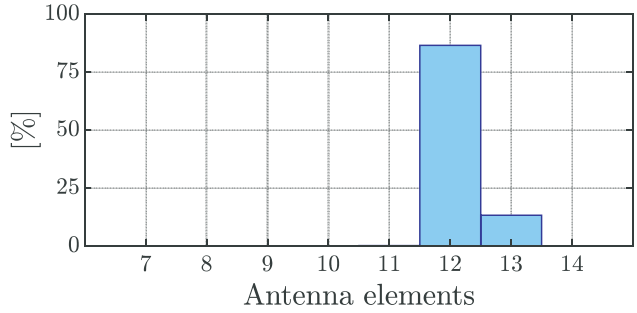

(c)

Figure 11. Distribution of the achieved lowly-correlated elements at every AS value. (a) Angular spread AS = 20. (b) Angular spread AS = 30. (c) Angular spread AS = 40.

9, 10, and 11, which account for 28%, 35%, and 23% of all considered incident directions. The minimum lowly-correlated number of elements is 7 which accounts for 1% of all considered incident directions, while the values of 8 and 12 occur with 9% and 4%, respectively.

The highest number of low-correlated elements is 12 elements (61%) at a 30° angular spread, followed by 11 elements (36%), and a few values of 10 elements (3%). Finally, when the angular spread is 40°, the highest number of low-correlated elements is reached, which is 13 elements (13%), but most of MIMO antenna size is 12 elements with 87% from the total values.

5. CONCLUSIONS

This work investigated the correlation between 14 elements of a sub-6 GHz for 5G mobile terminal. ECC is used as a figure of merit, and both uniform and directive Gaussian environments were considered. In a uniform environment, all ECC values are below the value of 0.15, which is much less than the required threshold. This indicates that the elements are low-correlated which leads to high capacity. However, the directive environments impact the ECC values rather differently. By linking the number of ECC values below the threshold of 0.3 and the number of low-correlated elements, it was found that even with an angular spread of 40°, the system is unable to achieve the ideal low-correlation between all 14 elements. The number of low-correlated elements at this AS is 12 with 87% and 13 elements with 13% from all considered incident directions. Results in this work showed that the Gaussian environment, which models the real propagation environment in cellular systems, limits the performance of massive MIMO for a mobile terminal even if a large number of antenna elements are lowly correlated in a uniform environment. This indicates the importance of accounting for the effect of the directive environment when evaluating the performance of future MIMO antenna designs.

ACKNOWLEDGMENT

The author would like to acknowledge the support from the Fundamental Research Grant Scheme (FRGS) under a grant number of FRGS/1/2019/TK04/UNIMAP/02/21 from the Ministry of Higher Education Malaysia, and the UniMAP Postdoctoral Fellowship.

REFERENCES

1. Kim, Y., et al., "Feasibility of mobile cellular communications at millimeter wave frequency," *IEEE J. Sel. Top. Signal Process.*, Vol. 10, No. 3, 589–599, 2016.
2. Shafique, K., B. A. Khawaja, F. Sabir, S. Qazi, and M. Mustaqim, "Internet of Things (IoT) for next-generation smart systems: A review of current challenges, future trends and prospects for emerging 5G-IoT scenarios," *IEEE Access*, Vol. 8, 23022–23040, 2020.
3. Fan, W., X. Carreño, P. Kyösti, and J. Ø. Nielsen, "Over-the-Air testing of MIMO-capable terminals," No. June, 38–46, 2015.
4. Rohani, B., K. Takahashi, H. Arai, Y. Kimura, and T. Ihara, "Improving channel capacity in indoor 4×4 MIMO base station utilizing small bidirectional antenna," *IEEE Trans. Antennas Propag.*, Vol. 66, No. 1, 393–400, 2018.
5. Ahmad, S., et al., "A compact CPW-fed ultra-wideband Multi-Input-Multi-Output (MIMO) antenna for wireless communication networks," *IEEE Access*, 2022.
6. Sharawi, M. S., "Current misuses and future prospects for printed multiple-input, multiple-output antenna systems [wireless corner]," *IEEE Antennas Propag. Mag.*, Vol. 59, No. 2, 162–170, 2017.
7. Sharawi, M. S., "Printed multi-band MIMO antenna systems and their performance metrics [wireless corner]," *IEEE Antennas Propag. Mag.*, Vol. 55, No. 5, 218–232, 2013.
8. Li, H., Z. T. Miers, and B. K. Lau, "Design of orthogonal MIMO handset antennas based on characteristic mode manipulation at frequency bands below 1 GHz," *IEEE Trans. Antennas Propag.*, Vol. 62, No. 5, 2756–2766, 2014.
9. Abdullah, M., et al., "High-performance multiple-input multiple-output antenna system for 5G mobile terminals," *Electronics*, Vol. 8, No. 10, 1090, 2019.
10. Ban, Y.-L., C. Li, G. Wu, and K.-L. Wong, "4G/5G multiple antennas for future multi-mode smartphone applications," *IEEE Access*, Vol. 4, 2981–2988, 2016.
11. Yang, Y., R. S. Blum, and S. Sfar, "Antenna selection for MIMO systems with closely spaced antennas," *EURASIP J. Wirel. Commun. Netw.*, Vol. 2009, 1–11, 2009.
12. Wong, K. and J. Lu, "3.6-GHz 10-antenna array for MIMO operation in the smartphone," *Microw. Opt. Technol. Lett.*, Vol. 57, No. 7, 1699–1704, 2015.
13. Deng, J., J. Yao, D. Sun, and L. Guo, "Ten-element MIMO antenna for 5G terminals," *Microw. Opt. Technol. Lett.*, Vol. 60, No. 12, 3045–3049, 2018.
14. Hu, W., et al., "Dual-band ten-element MIMO array based on dual-mode IFAs for 5G terminal applications," *IEEE Access*, Vol. 7, 178476–178485, 2019.
15. Li, Y., Y. Luo, and G. Yang, "12-port 5G massive MIMO antenna array in sub-6 GHz mobile handset for LTE bands 42/43/46 applications," *IEEE Access*, Vol. 6, 344–354, 2018.
16. Li, M.-Y., Y.-L. Ban, Z.-Q. Xu, J. Guo, and Z.-F. Yu, "Tri-polarized 12-antenna MIMO array for future 5G smartphone applications," *IEEE Access*, Vol. 6, 6160–6170, 2017.
17. Wang, H. and G. Yang, "Compact side-edge frame printed fourteen-element antenna array for triple-band MIMO operations in the 5G smartphone," *2019 International Conference on Microwave and Millimeter Wave Technology (ICMMT)*, 1–3, 2019.
18. Wong, K., J. Lu, L. Chen, W. Li, and Y. Ban, "8-antenna and 16-antenna arrays using the quad-antenna linear array as a building block for the 3.5-GHz LTE MIMO operation in the smartphone," *Microw. Opt. Technol. Lett.*, Vol. 58, No. 1, 174–181, 2016.

19. Tsai, C., K. Wong, and W. Li, "Experimental results of the multi-Gbps smartphone with 20 Multi-Input Multi-Output (MIMO) antennas in the 20 × 12 MIMO operation," *Microw. Opt. Technol. Lett.*, Vol. 60, No. 8, 2001–2010, 2018.
20. Zhao, K., Z. Ying, S. Zhang, and G. Pedersen, "User body effects on mobile antennas and wireless systems of 5G communication," *2020 14th European Conference on Antennas and Propagation (EuCAP)*, 1–5, 2020.
21. Buskgaard, E., A. Tatomirescu, S. C. Del Barrio, O. Franek, and G. F. Pedersen, "User effect on the MIMO performance of a dual antenna LTE handset," *2014 8th European Conference on Antennas and Propagation (EuCAP)*, 2006–2009, 2014.
22. Tian, R., B. K. Lau, and Z. Ying, "Multiplexing efficiency of MIMO antennas in arbitrary propagation scenarios," *2012 6th European Conference on Antennas and Propagation (EUCAP)*, 373–377, 2012.
23. Kyosti, P., "WINNER II channel models," *IST, Tech. Rep. IST-4-027756 Win. II D1. 1.2 V1. 2*, 2007.
24. Vasilev, I., V. Plicanic, and B. K. Lau, "Impact of antenna design on MIMO performance for compact terminals with adaptive impedance matching," *IEEE Trans. Antennas Propag.*, Vol. 64, No. 4, 1454–1465, 2016.
25. Guo, J., L. Cui, C. Li, and B. Sun, "Side-edge frame printed eight-port dual-band antenna array for 5G smartphone applications," *IEEE Trans. Antennas Propag.*, Vol. 66, No. 12, 7412–7417, 2018.
26. Li, Y., Y. Luo, and G. Yang, "Multiband 10-antenna array for sub-6 GHz MIMO applications in 5-G smartphones," *IEEE Access*, Vol. 6, 28041–28053, 2018.
27. Elshirkasi, A. M., et al., "Numerical analysis of users' body effects on a fourteen-element dual-band 5G MIMO mobile terminal antenna," *IEEE Access*, 2021.
28. Elshirkasi, A. M., et al., "Performance study of a MIMO mobile terminal with upto 18 elements operating in the sub-6 GHz 5G band with user hand," *IEEE Access*, Vol. 8, 28164–28177, 2020.
29. Jaglan, N., S. D. Gupta, and M. S. Sharawi, "18 element massive MIMO/diversity 5G smartphones antenna design for sub-6 GHz LTE bands 42/43 applications," *IEEE Open J. Antennas Propag.*, Vol. 2, 533–545, 2021.
30. Blanch, S., J. Romeu, and I. Corbella, "Exact representation of antenna system diversity performance from input parameter description," *Electron. Lett.*, Vol. 39, No. 9, 705–707, 2003.
31. Stjernman, A., "Relationship between radiation pattern correlation and scattering matrix of lossless and lossy antennas," *Electron. Lett.*, Vol. 41, No. 12, 1, 2005.
32. Sharawi, M. S., A. T. Hassan, and M. U. Khan, "Correlation coefficient calculations for MIMO antenna systems: A comparative study," *Int. J. Microw. Wirel. Technol.*, Vol. 9, No. 10, 1991–2004, 2017.
33. Azremi, A. A.-H., et al., "Coupling element-based dual-antenna structures for mobile terminal with hand effects," *Int. J. Wirel. Inf. Networks*, Vol. 18, No. 3, 146–157, 2011.
34. Elshirkasi, A. M., A. A. Al-Hadi, M. F. Mansor, R. Khan, and P. J. Soh, "Envelope correlation coefficient of a two-Port MIMO terminal antenna under uniform and Gaussian angular power spectrum with user's hand effect," *Progress In Electromagnetics Research C*, Vol. 92, 123–136, 2019.
35. Tounou, C. A., C. Decroze, D. Carsenat, T. Monediere, and B. Jecko, "Mobile communication antennas in uniform and Gaussian propagation channels," 2007.
36. Singh, H. S., B. R. Meruva, G. K. Pandey, P. K. Bharti, and M. K. Meshram, "Low mutual coupling between MIMO antennas by using two folded shorting strips," *Progress In Electromagnetics Research*, Vol. 53, 205–221, 2013.